Earthq Eng & Eng Vib (2022) 21: 53-65 **DOI**: https://doi.org/10.1007/s11803-021-2071-2

Discussion on blasting vibration monitoring for rock damage control in rock slope excavation

Yang Jianhua[1†], Cai Jiyong[1‡], Yao Chi[1§], Zhang Xiaobo[1†] and Liu Liansheng[2§]

1. *School of Civil Engineering and Architecture, Nanchang University, Nanchang 30031, China*

2. *School of Resource and Environmental Engineering, Jiangxi University of Science and Technology, Ganzhou 341000, China*

Abstract: Drill and blast is a commonly used method for rock slope excavation in hydropower engineering. During blasting excavation of rock slopes, far-field vibration monitoring on the first upper berm for statutory compliance is usually performed to control the blast-induced rock damage to the final slope face. In this study, for the rock slope excavation in the Jinping-I hydropower station, the field vibration monitoring and acoustic testing are presented to investigate the vibration characteristics on the first upper berm and the damage depth in the current bench. The relationship between the PPV on the first upper berm and the PPV damage threshold on the damage zone boundary is also studied through three-dimensional FEM simulations. The results show that on the first upper berm, the maximum vibration velocity component occurs in the vertical direction. While on the blasting damage zone boundary, the horizontal radial vibration velocity is the maximum component. For the Jinping-I slope with a bench height of 30 m, the radial PPV on the inner side of the first upper berm is 2.06% of the PPV threshold on the damage zone boundary. This ratio is increased as the bench height decreases. Therefore, the bench height of the rock slope is an important factor that cannot be ignored in determining the allowable vibration velocity for rock damage control.

Keywords: rock slope; blasting excavation; vibration; rock damage

1 Introduction

Hydropower stations are mostly built in areas of high mountains and deep valleys due to the large head fall of water. Construction of hydropower stations in these areas involves large-scale rock slope excavation. For example, in the Chinese Jinping-I hydropower station, the excavation height of the left-bank slope reaches up to 530 m and the excavation volume is 5.5 million m^3 (Sun *et al.*, 2018). It is one of the most complex rock slope projects for construction due to its complicated geology. In southwest China, there are many other artificially excavated high rock slopes, as listed in Table 1. The rock slopes play crucial roles in the construction and operation of the hydropower projects. In the construction stage, the rock slopes provide sites for arranging transportation routes, concrete mixing buildings and cable crane platforms. During the operation phase, the rock slopes undertake the tasks of supporting dams, resisting water thrust and preventing seepage. Therefore, the stability of the rock slopes will affect or even dominate the safety of the reservoir and dam system throughout the construction and operation periods (Zhou *et al*., 2016; Feng *et al*., 2019).

Drilling and blasting is the most widely adopted method for rock slope excavation in the hydropower engineering industry (Onederra *et al*., 2013; Yan *et al*., 2017; Liu *et al*., 2020; Hudaverdi and Akyildiz, 2021). When the drilling and blasting method is used, the stress waves and high-pressure gases produced by explosions will inevitably cause damage to the remaining rock mass of slopes (Bastante *et al*., 2012; Verma *et al*., 2018; Yuan *et al*., 2019; Yang *et al*., 2020). In addition, blast-induced seismic waves enable far-field rock discontinuities to open and slip, which can result in local or overall instability of slopes (Azizabadi *et al*., 2014; Huang *et al*., 2018). Due to the importance of the rock slopes to the reservoir and dam system, high standards of excavation quality are required for the rock slopes in hydropower projects. For this purpose, cautious blasting methods, such as pre-split blasting and smooth blasting, are usually employed, particularly in the zones near the slope profiles (Scarpato, 2016; Hu *et al*., 2018b).

During cautious blasting, there are two general methods that can be used to set the charge weight and

Correspondence to: Yao Chi, School of Civil Engineering and Architecture, Nanchang University, Nanchang 330031, China
Tel: +86-791-83969657
E-mail: chi.yao@ncu.edu.cn
[†]Associate Professor; [‡]Master Student; [§]Professor

Supported by: National Natural Science Foundation of China under Grant Nos. 51969015 and U1765207 and Jiangxi Provincial Natural Science Foundation under Grant Nos. 20192ACB21019 and 20204BCJ23002
Received January 1, 2020; **Accepted** July 12, 2021

distance for blastholes to reduce the blasting damage to the remaining rock masses. The first method is to account for the stress impact on the remaining rock mass, and the second method focuses on the vibration impact on the remaining rock mass (Blair, 2015b). The stress impact model makes a direct damage prediction based on a comparison between the peak stress and the rock strength. In this regard, Blair (2015b) justified the use of the maximum shear stress and the unconfined compressive strength. The vibration impact model predicts the peak particle velocity (PPV) based on the charge weight scaling law and makes a comparison with the PPV threshold of rock damage. These two methods have their advantages and disadvantages in attempting to quantify the blasting impacts (Blair, 2015b). However, the vibration impact model is more commonly used in practical rock blast projects for the control of blasting damage because it is easier to measure vibration velocity on site. In most blasting standards, the structure damage criteria are also given in terms of PPV limits (Singh and Roy, 2010; Karadogan *et al*., 2014).

The most direct method to establish the PPV threshold of rock damage is to actually damage the rock mass and record the resulting PPV. Based on vibration monitoring in combination with crack investigation or acoustic testing, many researchers have proposed the PPV damage thresholds for various kinds of rock masses. Holmberg and Persson (1978) claimed that the safety upper limit of PPV in hard bedrock was 70−100 cm/s. Bauer and Calder (1978) found that severe tensile cracks and some radial cracks were produced in the intact rock at a PPV of 63.5−254.0 cm/s. For competent granite in an underground mine, Ouchterlony *et al*. (1993) estimated blasting damage to occur at a PPV of 80 cm/s. On a test site with moderately jointed granitic gneiss, Yang *et al*. (1994) observed that a severe damage zone occurred when the PPV exceeded 200 cm/s. The measurements carried out by Blair and Armstrong (2001) and Brent *et al*. (2002) in dolerite showed that at a PPV of approximately 80 cm/s, a 10% change in rock volume occurred due to blasting damage. In a tunnel driven through compact basalt, Murthy and Dey (2003) concluded that the PPV level for overbreak to occur was more than 205 cm/s. For columnar jointed basalt in a dam foundation, Xia *et al*. (2020) found that obvious damage did not occur until the PPV reached about 50 cm/s.

The above studies indicate that the PPV threshold of rock damage is highly dependent on rock properties. With regard to common rock masses, the PPV threshold of rock damage is found to vary from 30 to 300 cm/s (Murthy and Dey, 2003). This is a very wide range and thus poses a challenge for practical blast projects to determine a precise PPV damage threshold. The vibration monitoring as close to the blasting damage zone as possible can only give a true picture of the PPV damage threshold. However, such near-field vibration monitoring is not widely carried out in the field because severe explosion stress waves and flying rocks may destroy monitoring equipment. In many blasting applications, vibration monitors are usually arranged in the far field for statutory compliance monitoring. With regard to blasting excavation of rock slopes, vibration monitors are typically placed on the upper berm surfaces (Azizabadi *et al*., 2014; Hu *et al*., 2018b; Haghnejad *et al*., 2019), as shown in Fig. 1. Then it is required that the PPV recorded on the first upper berm must not exceed the velocity limits stipulated in the standards or criteria (Singh and Roy, 2010; Karadogan *et al*., 2014). For example, in the Chinese safety regulation for blasting, the vibration velocity limits of permanent rock slopes are specified as 5–9 cm/s, 8–12 cm/s and 10–15 cm/s for different dominant frequencies $f \leq 10$ Hz, $10 < f \leq 50$ Hz and $f > 50$ Hz. Furthermore, this regulation also specifies that the PPV of the maximum velocity component is used to compare with the velocity limits.

Attempts to control the blasting damage through limiting the far-field PPV have been made by some researchers. Murthy and Dey (2003) assessed the PPV damage threshold levels by extrapolating the far-field

Table 1 High rock slopes of the hydropower projects in the southwest of China

Project name	Slope angle (°)	Natural slope height (m)	Excavation height (m)
Xiaowan	47	700−800	670
Dagangshan	>40	>600	380−410
Xiluodu	>60	300−350	300
Tianshenqiao	50	400	350
Xiangjiaba	>50	350	200
Baihetan	>42	440−860	280
Nuozhadu	>43	800	400−600
Wudongde	>43	830−1030	430

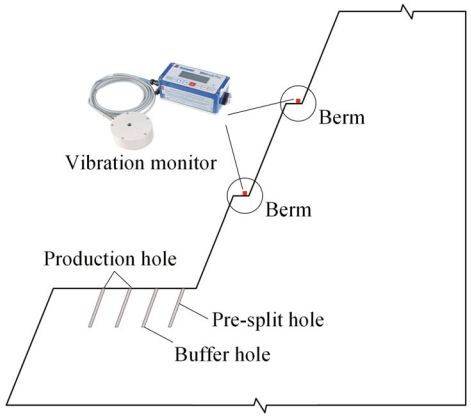

Fig. 1 Schematic diagram of the blasting vibration monitoring in a rock slope

PPV prediction equation to the near field. Li *et al*. (2011) and Zeng *et al*. (2018) established the statistical relationship between the rock damage depth and the PPV at 30 m distance for the blasting excavation of bedrock in nuclear power stations. For the blasts in rock slopes, Yan *et al*. (2016) and Hu *et al*. (2018a) developed the formulas between the rock damage depth in the current bench and the PPV on the upper bench face. Nevertheless, some important details have not been clarified with respect to the relationship between the rock damage to the current bench, the PPV threshold on the damage zone boundary and the PPV on the upper bench. Therefore, extra caution should be exercised when attempting to apply these statistical formulas to other sites.

In this study, for the blasting excavation of the rock slope in the Chinese Jinping-I hydropower station, the rock damage to the current bench and the vibration characteristics on the damage zone boundary and the upper bench berm are investigated. Based on this, some issues with regard to the far-field vibration monitoring for rock damage control are discussed. This case study is conducted by analyzing the vibration monitoring and acoustic testing data obtained in the field and also performing numerical simulations as a supplement. The numerical simulations are implemented by using the dynamic finite element software LS-DYNA.

2 Site description

2.1 General overview

The Jinping-I hydropower station is located on the main stream of the Yalong River in Sichuan Province, China. The water-retaining structure in this hydropower station is a double-curvature arch dam, as shown in Fig. 2. The height of the double-curvature arch dam is 305 m, and it is currently the highest double-curvature arch dam in the world. The arch spandrel groove, which is used to support the arch dam and bear the upstream water thrust, is artificially excavated by using the drilling and blasting method. The excavation height of the arch spandrel groove slope is 530 m on the left bank and 445 m on the right bank (Zhou *et al*., 2016). For the right-bank arch spandrel groove slope, its excavation is divided into several benches that have a height of 25−40 m and a slope ratio of 1:0.3. The berms with a width of 3.0 m are installed at the toe of each bench to provide access pathways.

The rock mass of the right-bank slope mainly includes striped marble and breccia marble. In addition, there are weaker greenschist interlayers continuously distributed in the striped marble. Geological surveys show that the rock mass located outside 40 m behind the natural slope face is fresh marble, classified into Class III_1−II in the Chinese rock classification system. The uniaxial compressive strength of the rock material is 60−75 MPa. The deformation modulus is 21−32 GPa for the Class II marble and 9−14 GPa for the Class III_1 marble. The Class II marble has an acoustic P-wave velocity exceeding 5500 m/s, and the P-wave velocity in the Class III_1 marble varies in a range from 4500 to 5500 m/s.

2.2 Excavation procedure and blasting parameters

In order to create a smooth slope profile and minimize blast-induced rock damage, the pre-split blasting method is employed in the excavation of the arch spandrel groove slope. The pre-split boreholes are 10−20 m in length and 90 mm in diameter. The spacing between the adjacent holes is 1.0 m. Decoupled charge configurations, which refer to leaving empty space between the explosive column and the blasthole wall, are used in the pre-split holes to reduce the borehole wall pressure. The charge used has a diameter of 32 mm and a total of 4.5−8.0 kg explosives are filled in a pre-split hole. For the purpose of controlling blasting disturbance, the pre-split boreholes are detonated in a millisecond-delay sequence. Each delay involves 6−10 pre-split boreholes and the maximum charge weight per delay is

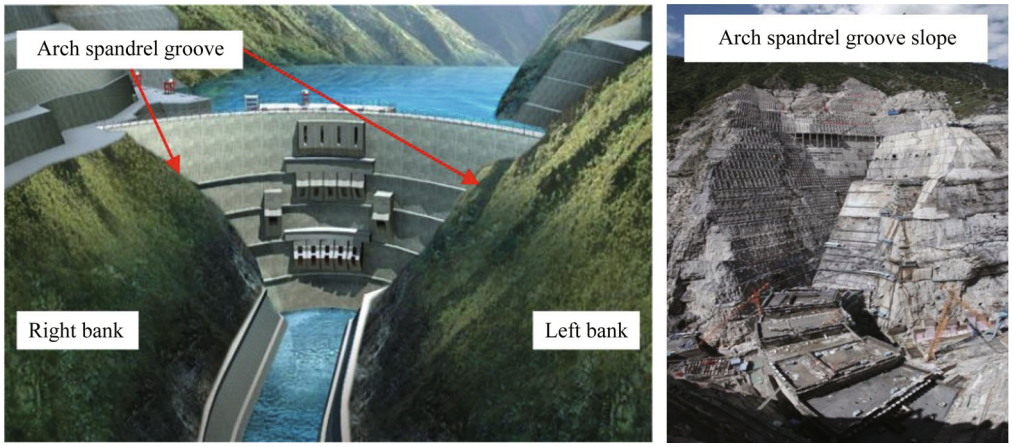

Fig. 2 Layout of Jinping-I hydropower station

limited within 48 kg. The delay interval between each group of pre-split boreholes is set to 50 ms. The pre-split boreholes are first detonated, followed by the production holes and buffer holes. The delay interval between the pre-split hole initiation and the production hole initiation is set to 440 ms. For the production hole and buffer hole blasts, a delay interval of 50 ms between holes and a delay interval of 110 ms between rows are designed. The production and buffer holes have a diameter of 110 mm and are filled with the explosives with a diameter of 70 mm. For the production blast, the maximum charge weight per delay is limited within 300 kg. For the buffer blast, a charge weight not exceeding 120 kg per delay is allowable. The used explosive is the emulsion-type explosive that has a density ranging 900−1300 kg/m^3 and a velocity of detonation in the range of 3000−5500 m/s.

Blasts of the pre-split boreholes generate a line of cracks through the designed slope profile prior to blasts of the production and buffer holes. The pre-splitting cracks play a role of preventing the stress waves produced by the production and buffer blasts from entering the final slope face. Under this circumstance, blast-induced damage to the slope face is mainly attributed to detonations of the pre-split holes (Hu *et al*., 2014). Therefore, in the following numerical simulations, only the pre-split hole blast is studied to improve computational efficiency.

3 Field tests

3.1 Blasting vibration monitoring

Blasting vibration monitoring has been carried out throughout the excavation process of the arch spandrel groove slope in the Jinping-I hydropower station. The vibration monitoring plays an important experimental role in any attempt to determine the rock mass and support responses to blast loading. During the blasting vibration monitoring, the observation points are typically arranged on the horizontal berms directly behind the blasting zone, as shown in Fig. 1. At each level, the distance between the observation point and the toe of the bench is approximately 1.0 m. That is, the observation points are located on the inner side of the berm at each level. The observation point on the first upper berm is generally taken as the control point where the vibration level is subject to statutory compliance.

The Instantel Minimate Plus vibration monitors are employed in the vibration velocity monitoring. At each observation point, a triaxial velocity sensor is installed to synchronously monitor horizontal radial, horizontal tangential and vertical vibration velocity components. The maximum velocity that the Instantel Minimate Plus vibration monitor can record is 254 mm/s, and its accuracy is 0.5 mm/s. The work frequency of the vibration monitor is in the range 2−250 Hz. The sampling rate is adjustable, ranging from 1 to 16 kHz. The particular sampling rate used in the field tests is 8 kHz.

The vibration monitoring data from 14 pre-split blasting tests and 45 production blasting tests are collected for the analysis in this study. Among these monitoring data, the horizontal distance from the blasting zone edges to the observation points varies between 3 and 47 m, and the vertical distance varies from 0 to 50 m. Figure 3 shows a typical vibration velocity history recorded on the first upper berm. It is clearly seen that among the three velocity components, the vertical component is maximum and the horizontal tangential component is minimum. In the 14 pre-split blasting tests, there are eight occurrences where the maximum velocity component occurs in the vertical direction. This event occurs 27 times with regard to the 45 production blasting tests, as counted in Fig. 4. This statistic indicates that on the first upper berm, the vertical vibration velocity is

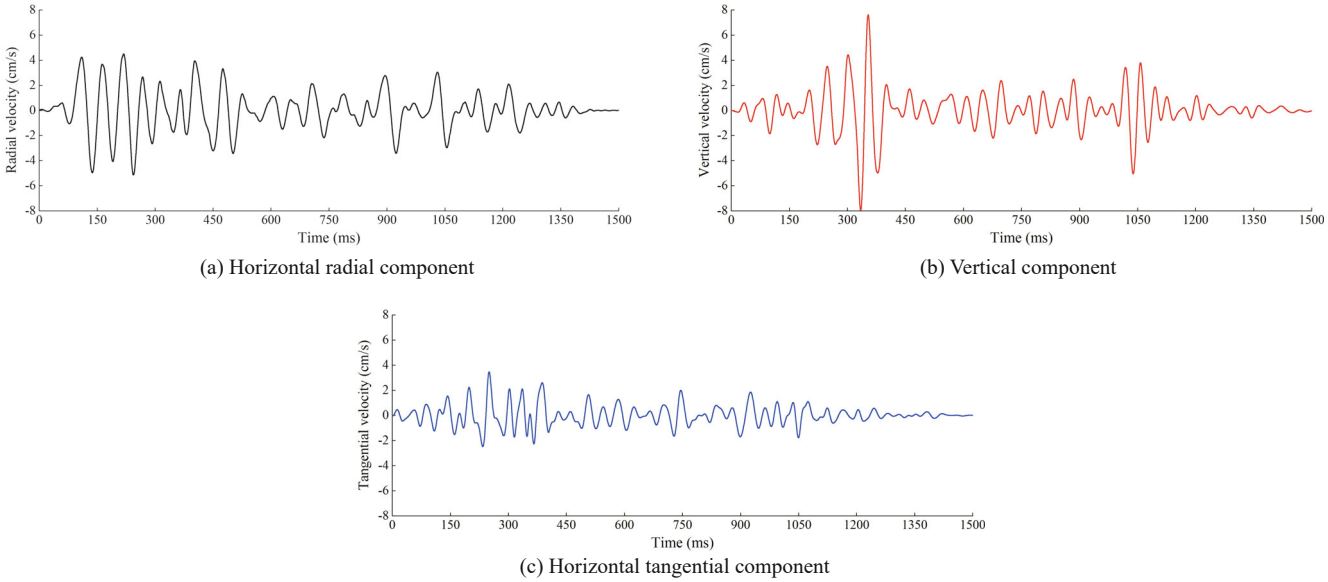

(a) Horizontal radial component

(b) Vertical component

(c) Horizontal tangential component

Fig. 3 Typical vibration velocity history recorded on the first upper berm

often the maximum velocity component.

Next, the vibration data monitored on the berms at other elevations are also incorporated for further statistical analysis. Due to the difficulty of blasting vibration prediction, it is assumed that the *PPV* of blasting vibration follows the typical charge weight scaling law:

$$PPV = K \cdot \left(d/\sqrt{W}\right)^{-\alpha} \tag{1}$$

where *PPV* is the peak particle velocity in m/s, d is the distance from the blasting source to the vibration observation point in m, W is the maximum charge weight per delay in kg, and K and α are site constants. In this study, long cylindrical charges are used in the bench blasts, and hence the distance is scaled with the square root of the charge weight (Leidig *et al*., 2010).

In a strict sense, the scaling law in Eq. (1) is not a fundamental equation for blasting vibration prediction despite its popular application (Blair, 2004). A problem of particular concern is that such a scaling law is dimensionally unsound. Perhaps the best way to view Eq. (1) is that it provides a pragmatic means of scaling vibration data under a given charge weight and distance. Since it lacks real physical meaning, the vibration attenuation in the horizontal direction and that in the vertical direction are not considered separately. The slant distance between the blasting source and the monitoring point is used in Eq. (1) for curve fitting. Using the data measured on the berms at different elevations during the 14 pre-split blasting tests, Fig. 5 shows the *PPV* versus scaled distance on a log-log plot for the three vibration velocity components. Based on these data, simple linear regression analyses are conducted to obtain the *PPV* attenuation relationships with distance, as shown in Fig. 5. The slope of the best-fit straight line gives the exponent α, and the intercept at $d/\sqrt{W}=1$ gives the logarithm of the coefficient K. For the horizontal radial velocity component,

$$PPV_{\mathrm{R}} = 0.0864 \cdot \left(d/\sqrt{W}\right)^{-1.16} \tag{2}$$

for the horizontal tangential velocity component,

$$PPV_{\mathrm{T}} = 0.0705 \cdot \left(d/\sqrt{W}\right)^{-1.08} \tag{3}$$

and for the vertical velocity component,

$$PPV_{\mathrm{V}} = 0.1624 \cdot \left(d/\sqrt{W}\right)^{-1.33} \tag{4}$$

The above attenuation relationships also indicate that for the blasting vibration on the upper berms of the slope, the vertical velocity component is greater than the horizontal radial and tangential components. Note that the above scaling laws are derived from 39 sets of data of the 14 blasting tests. These data may be insufficient to derive a precise statistical law. In addition, there is a scatter for the field data shown in Fig. 5. This scatter is probably due to some uncertain factors, such as rock discontinuities on wave propagation paths, rock looseness at monitoring locations and instrument differences at various measurement points. Because of the limited and scattered field data, an appropriate statistical analysis needs to be conducted to demonstrate there are statistical differences between any two of the three velocity components. To achieve this purpose, hypothesis tests of robust regression are carried out on the field data shown in Fig. 5 by using the software package SPSS. The first test is to determine whether there is a significant difference between the slopes of any two fitted lines; and the next test is to determine if the intercepts of the two lines are significantly different. Only when the slopes and the intercepts are both significantly different, it is considered that there is a statistical difference between the two fitted lines. The hypothesis tests show that at the significance level s=0.05, there is a significant difference between the radial component and the vertical component, and also between the tangential component and the vertical component. However, there is no significant difference

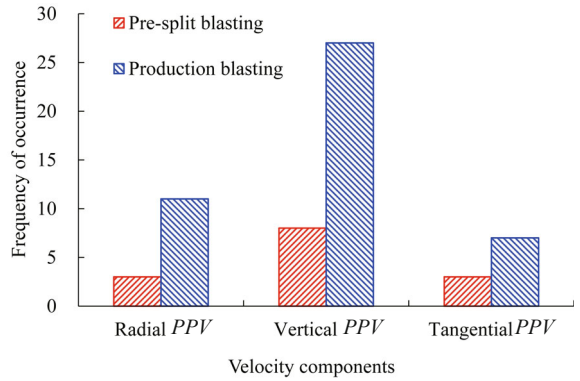

Fig. 4 Statistics of the maximum velocity component recorded on the first upper berm

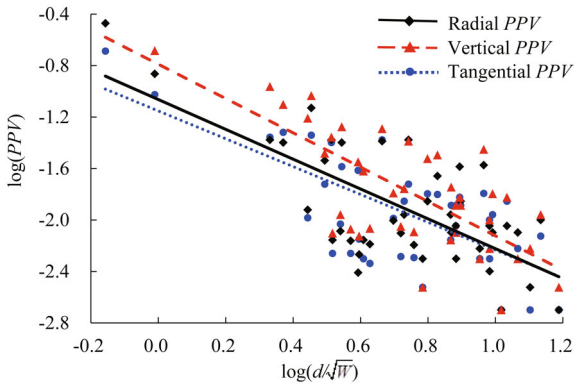

Fig. 5 *PPV* fitting for the vibration velocities monitored on the berms at different elevations

between the radial and tangential components. Through the statistical tests, it is meaningful to claim that the vertical velocity is the maximum vibration velocity component on the upper berms.

In accordance with the standards similar to the Chinese safety regulation for blasting, the *PPV* of the vertical vibration component must not exceed the vibration limits stipulated in the standards. Notably, in the field blasting tests in this study, all the vibration observation points are arranged in the far field for statutory compliance monitoring. Therefore, the conclusion obtained above may not be applicable to the near-field vibration.

3.2 Blasting damage testing

In the near field of blasting, rock damage is inevitably induced due to excessive vibration. As mentioned earlier, when the pre-split blasting technology is used, the blast-induced rock damage to the slope face is mainly attributed to the detonation of the pre-split holes. Under the framework of blasting vibration monitoring, the most direct method of rock damage assessment is to record the near-field *PPV* and then compare it with the *PPV* threshold of rock damage. However, for this direct method, there is a high risk of destroying the monitoring instrument in the near field caused by explosion stress waves or flying rocks. Because of this, the near-field vibration monitoring close to the blasting damage zone is not carried out in the field tests. Fortunately, there are many other ways to detect blast-induced rock damage, such as acoustic testing, seismic tomography, digital borehole camera, borehole core logging and hydraulic pressure testing (Agan, 2016; Guo *et al*., 2017; Wang *et al.*, 2019; Yang *et al*., 2020). Among these methods, acoustic testing is widely used in rock slope projects due to its convenient operations, lower costs and higher precision. During blasting excavation of the Jinping-I arch spandrel groove slope, acoustic testing is performed after blasting of the last bench at each level to assess the depth and degree of the rock damage behind the final slope face.

After blasting of the last bench, three acoustic test holes are drilled perpendicularly into the rock mass behind the slope face. The length of the acoustic test holes is approximately 4 m and the diameter is 90 mm. In each test, the three acoustic holes are arranged in an equilateral triangle with spacing of 1.2−1.5 m apart from each other, as shown in Fig. 6. The single-hole method is employed and the testing is carried out sequentially in the three acoustic holes. The testing equipment mainly consists of a data logger, a transmitting transducer and a receiving transducer. The transducers move up from the bottom of the test holes and the logger records the data at an interval of 0.2 m. Figure 7(a) presents the P-wave velocities at different depths in the rock mass measured from five acoustic tests. The five tests are performed at different elevations but in the same type of rock mass, i.e., Class III_1 marble.

Because the velocity of the acoustic wave propagation in rock masses is affected by many factors, the data measured in different test holes and on different benches show a certain degree of scatter. Nevertheless, it still can be seen that the P-wave velocity of the rock mass within 1.6 m depth behind the slope face is obviously lower than that of the rock mass located inside. This indicates that the blasting construction causes damage to the rock mass beyond the designed slope profile. Taking the average of the data tested at the same depth, the variation of the P-wave velocity with increasing depth is shown in Fig. 7(b). The average P-wave velocity first keeps increasing within 1.6 m distance and then gradually tends to a relatively stable value. This stable value can be considered as the P-wave velocity of the undamaged rock mass, approximately 4850 m/s in our tests. It falls within the range of 4500−5500 m/s that is officially recommended. When the P-wave velocity is lower than the undamaged value, the rock mass is considered to be damaged by blasting. According to this convention, the depth of the blast-induced damage zone is 1.6–2.0 m.

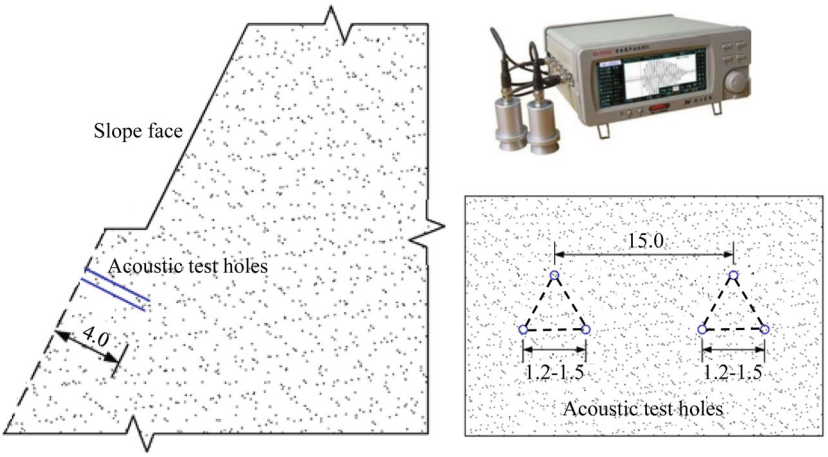

Fig. 6 Arrangement of acoustic test holes for the blasting damage testing (units: m)

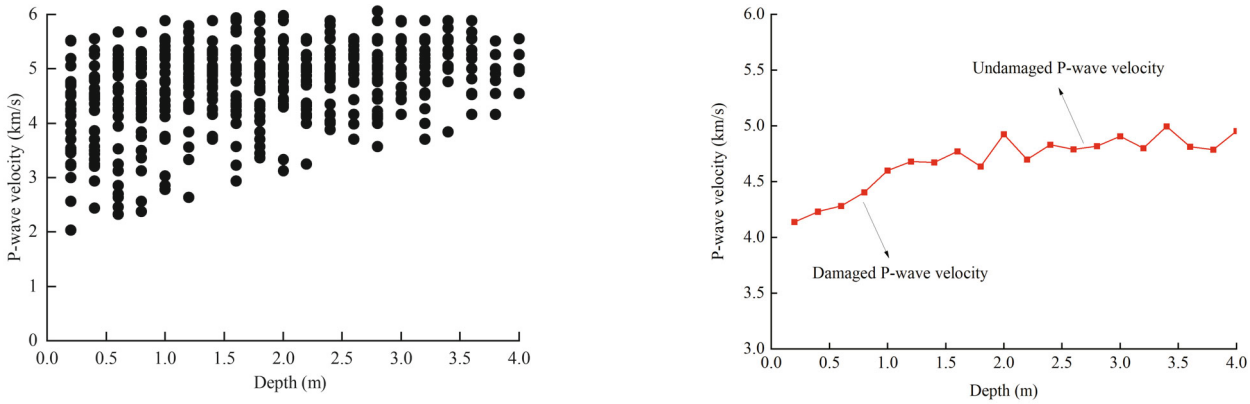

(a) Discrete data (b) Average P-wave velocities

Fig. 7 Acoustic P-wave velocities measured at different depths in the slope

4 Numerical simulation of rock damage and vibration

Because the vibration monitors are not installed beneath the slope surface for the near-field monitoring, it is difficult from the field tests to determine the *PPV* threshold of rock damage. Furthermore, because the monitors are typically located on the berms, the relationship between the vibration in the near field for rock damage and the vibration on the upper berms for statutory compliance is not easy to figure out. Therefore, in order to correlate the far-field vibration monitoring and the near-field rock damage control, it is necessary to conduct related numerical simulations. In this section, the blast of the pre-split holes is simulated to simultaneously observe the near-field vibration for rock damage and the far-field vibration for statutory compliance.

4.1 Numerical model

The dynamic finite element software LS-DYNA is employed to simulate the blast of the pre-split holes. LS-DYNA has proven to be one of the few codes that can simulate explosive detonations and the interactions between explosives and structures. It is well known that the accuracy of any dynamic FEM modeling is highly dependent on the relative size of the finite elements compared with the shortest wavelength. In this regard, Blair (1985) concluded that 6−12 elements per wavelength were required to avoid any wave distortion. The shortest wavelength of interest can be estimated through multiplying the lowest wave velocity (Rayleigh wave velocity) by the rise time of the blasting load. The Rayleigh wave velocity of 1800 m/s and the rise time of 0.1 ms give the shortest wavelength of 0.18 m. Consequently, in order to resolve the high-frequency waves in the near field, a uniform mesh with the element size smaller than 0.03 m is the optimum arrangement. If all the elements remain uniform at a size smaller than 0.03 m, the numerical model will require at least 92.5 million elements to cover a 50×50×1 m^3 volume. Clearly, it is too time-consuming or even infeasible to perform such a refined three-dimensional simulation. Since the wavelength becomes longer gradually with an increase in the distance from the blastholes, graded elements are used in the far field.

According to the geometry of the Jinping-I arch spandrel groove slope, an axisymmetric rock slope model with two pre-split blastholes is developed, as shown in Fig. 8. The diagram on the left side is the cross-sectional view of the whole model, and the diagram on the right side is the isometric view of the mesh around the pre-split blastholes. The numerical model measures 50×90×1 m^3, including three benches. Each bench has a height of 30 m and a slope ratio of 1:0.3. The berms between the adjacent benches are 3 m in width. The pre-split blastholes are arranged in the bench that is currently being excavated, and they have a height of 10 m and a diameter of 90 mm. In the region of 5 m surrounding the blastholes, the model is discretized into a mesh of hexahedral elements with a side length of 0.03 m. Outside this region, the graded elements to the outer boundaries are used. The entire model consists of 3.94 million elements. Free boundary conditions are applied to the slope face, and symmetric boundaries are enforced on the front and back faces. The other

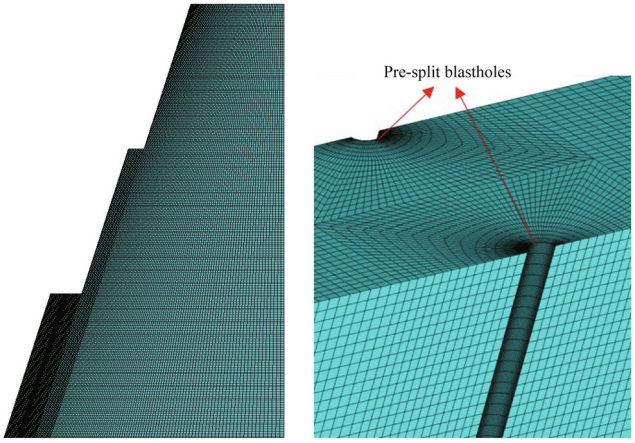

Fig. 8 Dynamic FEM model used in the numerical simulations

exterior boundaries are set to be non-reflective to reduce unwanted reflections from the finite boundaries. In this numerical study, rock discontinuities such as fissures and faults are not considered.

4.2 Material models

The material system of this numerical study involves explosive, air and rock. In the fluid-structure interaction analysis, the Arbitrary Lagrangian-Eulerian (ALE) solver is used to handle the explosive and air materials, and the Lagrange solver is used to handle the rock material. The interaction between the ALE mesh and the Lagrange mesh is achieved by the keywords '*CONSTRAINED_LAGRANGE_IN_SOLID'.

In LS-DYNA, simulation of explosive detonations is achieved by the Jones–Wilkins–Lee (JWL) equation of state (EOS). The JWL EOS describes the pressure change due to the expansion of detonation products for high explosives. It is written in the form:

$$p = C_1\left(1-\frac{\omega}{R_1V}\right)\mathrm{e}^{-R_1V} + C_2\left(1-\frac{\omega}{R_2V}\right)\mathrm{e}^{-R_2V} + \frac{\omega E_\mathrm{d}}{V} \quad (5)$$

where p is the pressure of the detonation products, V is the relative volume, E_d is the specific energy, and C_1, C_2, R_1, R_2 and ω are explosive constants. These explosive constants of the JWL equation is determined by experiments. Sanchidrian *et al*. (2015) determined the JWL parameters of emulsion explosives by using the cylinder tests. During the tests, the adiabatic expansion process of the detonation products was obtained through measuring the motion of the cylinder wall. According to the tests of Sanchidrian *et al*. (2015), the adopted JWL constants are summarized in Table 2.

In the numerical modeling, the air is considered as an ideal gas and is simulated by using the null material model in a polynomial EOS. The air pressure P_a is defined as:

Table 2 JWL EOS parameters of the explosive used in the numerical simulations

Parameters	Value
Density ρ_e, kg/m^3	1130
Velocity of detonation *VOD*, m/s	6031
CJ pressure P_CJ, GPa	9.558
Parameter C_1, GPa	365.3
Parameter C_2, GPa	2.703
Parameter R_1	4.99
Parameter R_2	0.892
Parameter ω	0.23
Detonation energy per unit volume E_0, GPa	3.036

$$P_\mathrm{a} = A_0 + A_1\mu + A_2\mu^2 + A_3\mu^3 + (A_4 + A_5\mu + A_6\mu^2)e \quad (6)$$

where e is the internal energy per unit volume, A_0, A_1, A_2, A_3, A_4, A_5 and A_6 are constants, and $\mu=\rho/\rho_0-1$, in which ρ and ρ_0 refer to the current density and the initial density. For an ideal gas, the material constants are set as $A_0=A_1=A_2=A_3=A_6=0$ and $A_4=A_5=0.40$. The initial destiny of air ρ_0 is 1.29 kg/m^3, and the initial internal energy per unit volume e_0 is 0.25 J/cm^3 (Wang *et al*., 2006).

In the present study, the Johnson-Holmquist (J-H) constitutive model is used to simulate the rock behavior under blast loading. The J-H model is pressure and strain rate dependent, and is suitable for modeling high pressure, large strain and high strain rate problems of brittle materials such as rock (Johnson and Holmquist, 1994; Ma and An, 2008). It consists of a representation of the intact and fractured material strength, a pressure-volume relationship and a damage model that describes the material from an intact state to a fully fractured state. The evolution from the intact state to a fractured state is represented by a damage scalar D ($0\le D\le 1.0$).

At the intact state (D=0), the normalized material strength is defined as σ_i^*,

$$\sigma_\mathrm{i}^* = A\left(P^*+T^*\right)^N\left(1+C\ln\dot{\varepsilon}^*\right) \quad (7)$$

At the fully fractured state (D=1), the normalized material strength is given by σ_f^*,

$$\sigma_\mathrm{f}^* = B\left(P^*\right)^M\left(1+C\ln\dot{\varepsilon}^*\right) \quad (8)$$

The normalized strength of the fractured material at $0<D<1$ is expressed as σ^*:

$$\sigma^* = \sigma_\mathrm{i}^* - D\left(\sigma_\mathrm{i}^* - \sigma_\mathrm{f}^*\right) \quad (9)$$

In Eqs. (7)–(9), A, N, C, B and M are material constants, and P^*, T^* and $\dot{\varepsilon}^*$ are the normalized pressure, hydrostatic tensile strength and strain rate. These quantities are normalized by $\sigma_\mathrm{i}^*=\sigma_\mathrm{i}/\sigma_\mathrm{HEL}$, $\sigma_\mathrm{f}^*=\sigma_\mathrm{f}/\sigma_\mathrm{HEL}$, $\sigma^*=\sigma/\sigma_\mathrm{HEL}$, $P^*=P/P_\mathrm{HEL}$, $T^*=T/P_\mathrm{HEL}$ and $\dot{\varepsilon}^*=\dot{\varepsilon}/\dot{\varepsilon}_0$, in which σ_i and σ_f are the actual strength of the intact material and the fully fractured material, σ is the actual equivalent stress, P is the actual pressure, T is the actual hydrostatic tensile strength, σ_HEL and P_HEL are the equivalent stress and the pressure at the Hugoniot elastic limit (HEL), $\dot{\varepsilon}$ is the actual equivalent strain rate, and $\dot{\varepsilon}_0$ is the reference strain rate to which the value 1.0 s^{-1} is assigned.

A polynomial EOS is used in the J-H model to describe the relationship between the pressure P and the compression variable μ_r:

$$P = k_1\mu_\mathrm{r} + k_2\mu_\mathrm{r}^2 + k_3\mu_\mathrm{r}^3 + \Delta P \quad (\mu_\mathrm{r}\ge 0) \quad (10)$$

where k_1, k_2 and k_3 are material constants (k_1 is the bulk modulus), and ΔP is an additional pressure increment determined from the energy consideration. The hydrostatic potential energy corresponding to the pressure increment is converted from the elastic energy loss due to a decrease in the deviator stress. The amount of conversion is controlled by a fraction β ($0 \le \beta \le 1$). The compression variable μ_r is defined as $\mu_r = \rho_r / \rho_{r0} - 1$, in which ρ_r is the current rock density and ρ_{r0} is the initial rock density. For the tension case at $\mu_r < 0$, Eq. (10) is replaced by $P = k_1 \mu_r$.

In the J-H model, material damage begins to accumulate when the material undergoes plastic deformation. The damage scalar D is calculated by:

$$D = \sum \frac{\Delta \varepsilon_p}{\varepsilon_p^f} \tag{11}$$

where $\Delta \varepsilon_p$ is the increment in the equivalent plastic strain during a calculation cycle, and ε_p^f is the equivalent plastic strain to fracture under a constant pressure P. The fracture strain in this model is obtained from:

$$\varepsilon_p^f = D_1 \left(P^* + T^* \right)^{D_2} \tag{12}$$

where D_1 and D_2 are damage constants.

A group of J-H model parameters need to be determined in the LS-DYNA modeling. These parameters include elastic constants, strength constants, pressure constants and damage constants. The rock mass of the Jinping-I arch spandrel groove slope is mainly composed of marble. Based on the laboratory tests on the Jinping marble and the procedures that determine the J-H model parameters (Ai and Ahrens, 2006; Banadaki and Mohanty, 2012), the adopted rock constants in the numerical simulations are summarized in Table 3. The damage constants D_1 and D_2 are not directly measurable, and thus numerical adjustments are performed. It is found that D_1=0.005 and D_2=0.7 can achieve an acceptable rock damage pattern.

5 Numerical results and discussion

Figure 9 shows the simulated rock damage to the remaining rock mass of the slope caused by the pre-split blast. The right side of this figure is an expanded view of the blasting damage zone. The rock mass in the immediate vicinity of the blastholes is fully fractured and the damage scalar D is equal to 1.0. As the explosion stress waves attenuate with increasing distance, the degree of rock damage is gradually reduced. At the distance of 1.7 m behind the designed slope face, the damage scalar D has declined to zero. Therefore, in the numerical simulation, the depth of the blasting damage zone is 1.7 m. It agrees well with the field result determined by using the acoustic testing method. Beyond the blasting damage zone, the explosion seismic waves or vibration do not have enough energy to damage the slope rock mass. In theory, the *PPV* of the vibration on the boundary between the damaged zone and the undamaged zone is the *PPV* threshold for initiation of blast-induced rock damage. In this numerical study, the vector *PPV* damage threshold is about 260 cm/s, which falls in the range of 30 to 300 cm/s that Murthy and Dey (2003) concluded. However, as mentioned earlier, the near-field vibration nearby the damage zone boundary is infrequently monitored in the field due to the risk of instrument destruction from excessive vibration. Because of this, during practical blasting design, the *PPV* threshold on the damage zone boundary is generally not used as the velocity limit of damage control. Instead, limiting the vibration velocity on the first upper berm becomes a more practical approach for blasting vibration monitoring to control the rock damage to the current bench (Yan *et al*., 2016; Hu *et al*., 2018a). Under this scenario, it is necessary to clarify the relationship between the vibration velocity on the damage zone boundary and the vibration velocity on the first upper berm.

In order to track the change of the vibration velocity, a series of observation points are arranged on the numerical model, as presented in Fig. 10. Nos. 1−5 observation points are arranged on the boundary of the blasting damage zone. Nos. 6−10 and Nos. 21−25 observation points are located on the surfaces of the current berm and the first upper berm. The other observation points are placed on the slope face between the two berms. In the far field, the surface waves are expected to dominate (Blair, 2015a; Yang *et al*., 2019). Therefore, in the far field, only the vibration on the slope and berm surfaces is investigated in this numerical study.

Figure 11 presents the variation of the *PPV* from the damage zone boundary to the first upper berm. The *PPV* on the damage zone boundary is almost constant. On the surface of the current berm, the vibration velocity drops sharply with an increase in the horizontal distance.

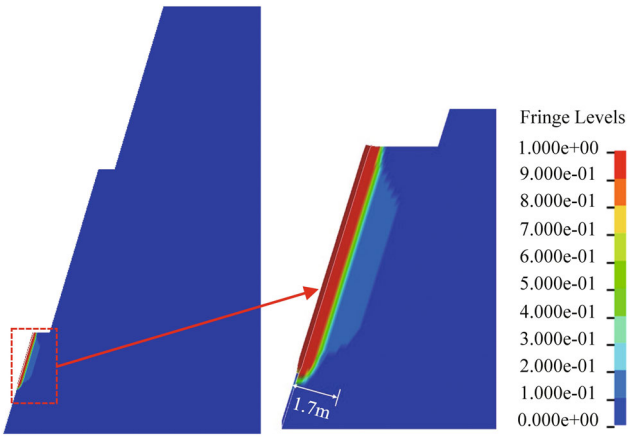

Fig. 9 Distribution of the blasting damage zone

On the slope face, the vibration velocity first gradually decreases and then locally increases at the tip due to the whipping effect. In this local zone, the *PPV* at the outer edge of the first upper berm (No. 21 observation point) reaches a maximum value. Along the first upper berm, the vibration amplitude decreases again as the distance increases. At the toe of the first upper bench, the *PPV* decays to a level equal to the value before the local increase. At farther distance, the vibration will continue to decrease. Therefore, in order to avoid the whiplash effect, the vibration monitors should be installed on the inner side of the first upper berm for compliance monitoring.

Table 3 J-H parameters of the rock material used in the numerical simulations

Parameters	Value
Density ρ_{r0}, kg/m^3	2700
Poisson's ratio v	0.22
Young's modulus E, GPa	25
Shear modulus G, GPa	10.25
Pressure coefficient k_1, GPa	14.88
Pressure coefficient k_2, GPa	-18
Pressure coefficient k_3 , GPa	3980
Hugoniot elastic limit *HEL*, GPa	4.5
HEL pressure P_{HEL}, GPa	3.44
HEL equivalent stress σ_{HEL}, GPa	1.58
Hydrostatic tensile limit T, MPa	8
Intact strength parameter A	0.72
Intact strength parameter N	0.61
Fractured strength parameter B	0.24
Fractured strength parameter M	0.61
Normalized maximum fracture strength $\sigma^*_{f\,max}$	0.25
Strain rate parameter C	0.005
Bulk factor β	0.50
Damage coefficient D_1	0.005
Damage exponent D_2	0.7

In this numerical study, the radial *PPV* threshold on the blasting damage zone is about 252.8 cm/s. At the bench height of 30 m, the radial *PPV* on the inner side of the first upper berm is approximately 5.2 cm/s, 2.06% of the *PPV* damage threshold. The cases with a bench height of 20 m and 15 m are also simulated in this section. In these simulations, the blasting and material parameters remain the same as above. When the bench height is reduced to 20 m, the radial *PPV* on the inner side of the first upper berm increases to 8.3 cm/s, 3.28% of the *PPV* damage threshold, as shown in Fig. 12. The ratio reaches 4.95% as the bench height is further reduced to 15 m. It is clearly seen that the relationship between the *PPV* on the first upper berm and the *PPV* threshold on the damage zone boundary is closely related to the height of the upper bench. Therefore, the influence of the upper bench height cannot be ignored in determining the vibration limits on the first upper berm. For a slope with a smaller bench height, a greater vibration velocity is allowed to occur on the inner side of the first upper berm under the same damage condition (the same *PPV* damage threshold).

According to the numerical simulation results in Figs. 11 and 12, the vertical velocity is the maximum vibration velocity component at the observation points on the first upper berm. This demonstrates the statistical result of the field monitoring data analyzed in Section 3.1. In the standards similar to the Chinese safety regulation for blasting, it is stated that the maximum vibration velocity component must not exceed the velocity limits specified in the standards. Based on the above field

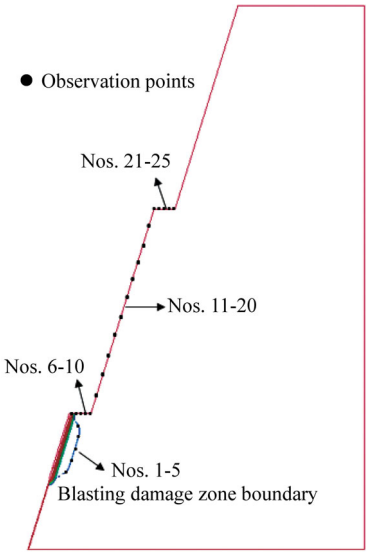

Fig. 10 Arrangement of the observation points in the numerical analysis

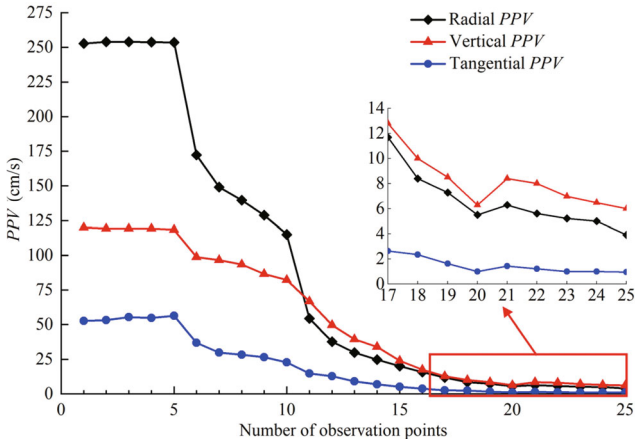

Fig. 11 *PPV* variation from the damage zone boundary to the first upper berm at the bench height of 30 m

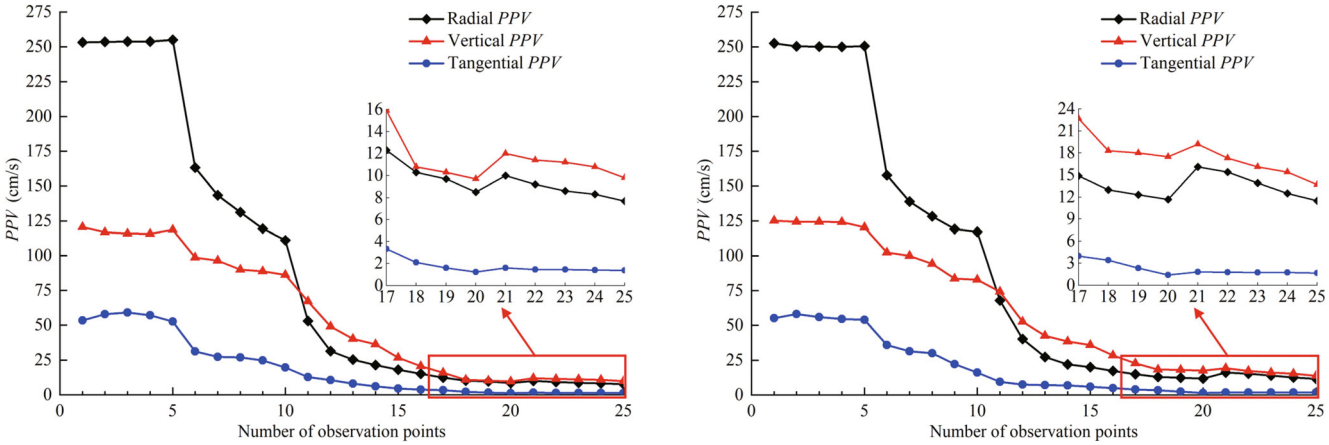

Fig. 12 *PPV* variation from the damage zone boundary to the first upper berm at different bench heights

surveys and numerical simulations, more specifically, it is the *PPV* of the vertical vibration component that must comply with the specified velocity limits. Note that on the blasting damage zone boundary, the radial vibration velocity component is much higher than the vertical and tangential components. The vector *PPV* in the near field is dominated by the radial velocity component. With regard to this point, it is different from the vibration on the first upper berm.

6 Conclusions

For the excavation of the Jinping-I arch spandrel groove slope, the blast-induced rock damage to the current bench and the vibration velocities on the damage zone boundary and the first upper berm were investigated by using site surveys and three-dimensional FEM simulations. It is found that on the first upper berm, the vertical vibration velocity is the maximum velocity component. Therefore, more specifically, it is the PPV of the vertical vibration component that must not exceed the velocity limits specified in the standards similar to the Chinese safety regulation for blasting. In order to avoid the whiplash effect, vibration monitors are preferably installed on the inner side of the upper berm for the compliance monitoring. The relationship between the PPV on the first upper berm and the PPV damage threshold on the damage zone boundary is dependent on the height of the upper bench. In determining the allowable vibration velocity on the first upper berm, the height of the upper bench is an important factor that cannot be ignored.

Blast-induced damage and vibration on rock slopes is a very complicated issue, affected by many factors such as explosive properties, blasthole arrangements, detonation sequences, rock properties and slope geometry. Because of this, the blasting vibration velocity limits in the current standards for rock damage control are mostly semi-empirical, based on extensive monitoring data at different sites. In order to accurately determine the allowable vibration velocity of the compliance monitoring, further studies in theory and simulation are required to reveal the relationship between the vibration on the upper berm and the vibration on the damage zone boundary.

Acknowledgment

This work is supported by the National Natural Science Foundation of China (Grant Nos. 51969015 and U1765207) and the Jiangxi Provincial Natural Science Foundation (Grant Nos. 20192ACB21019 and 20204BCJ23002). The authors wish to express their thanks to the sponsors for this support.

References

Agan C (2016), "Prediction of Squeezing Potential of Rock Masses Around the Suruc Water Tunnel," *Bulletin of Engineering Geology and the Environment*, **75**(2): 451–468.

Ai HA and Ahrens TJ (2006), "Simulation of Dynamic Response of Granite: A Numerical Approach of Shock-Induced Damage Beneath Impact Craters," *International Journal of Impact Engineering*, **33**(1): 1–10.

Azizabadi HRM, Mansouri H and Fouche O (2014), "Coupling of Two Methods, Waveform Superposition and Numerical, to Model Blast Vibration Effect on Slope Stability in Jointed Rock Masses," *Computers and Geotechnics*, **61**: 42–49.

Banadaki DMM and Mohanty B (2012), "Numerical Simulation of Stress Wave Induced Fractures in Rock," *International Journal of Impact Engineering*, **40**: 16–25.

Bastante FG, Alejano L and Cao JG (2012), "Predicting the Extent of Blast-Induced Damage in Rock Masses," *International Journal of Rock Mechanics and Mining Sciences*, **56**: 44–53.

Bauer A and Calder PN (1978), "Open Pit and Blast

Seminar," *Course No. 63221*, Mining Engineering Department, Queens University, Kingston, Ontario, Canada.

Blair DP (1985), "Acoustic Pulse Transmission in Half-Spaces and Finite-Length Cylindrical Rods," *Geophysics*, **50**(11): 1676–1683.

Blair DP (2004), "Charge Weight Scaling Laws and the Superposition of Blast Vibration Waves," *Fragblast*, **8**(4): 221–239.

Blair DP (2015a), "The Free Surface Influence on Blast Vibration," *International Journal of Rock Mechanics and Mining Sciences*, **77**: 182–191.

Blair DP (2015b), "Wall Control Blasting," *Proceedings of the 11th International Symposium on Rock Fragmentation by Blasting*, Sydney, Australia, 13–26.

Blair DP and Armstrong LW (2001), "The Influence of Burden on Blast Vibration," *Fragblast*, **5**(1–2): 108–129.

Brent GF, Smith GE and Lye GN (2002), "Studies on the Effect of Burden on Blast Damage and the Implementation of New Blasting Practices to Improve Productivity at KCGMs Fimiston Mine," *Fragblast*, **6**(2): 189–206.

Feng XT, Zhou YY and Jiang Q (2019), "Rock Mechanics Contributions to Recent Hydroelectric Developments in China," *Journal of Rock Mechanics and Geotechnical Engineering*, **11**(3): 511–526.

Guo HS, Feng XT, Li SJ, Yang CX and Yao ZB (2017), "Evaluation of the Integrity of Deep Rock Masses Using Results of Digital Borehole Televiewers," *Rock Mechanics and Rock Engineering*, **50**(6): 1371–1382.

Haghnejad A, Ahangari K, Moarefvand P and Goshtasbi K (2019), "Numerical Investigation of the Impact of Rock Mass Properties on Propagation of Ground Vibration," *Natural Hazards*, **96**(2): 587–606.

Holmberg R and Persson PA (1978), "The Swedish Approach to Contour Blasting," *Proceedings of the 4th Conference on Explosive and Blasting Technique*, New Orleans, USA, 113–127.

Hu YG, Liu MS, Wu XX, Zhao G and Li P (2018a), "Damage-Vibration Couple Control of Rock Mass Blasting for High Rock Slopes," *International Journal of Rock Mechanics and Mining Sciences*, **103**: 137–144.

Hu YG, Lu WB, Chen M, Yan P and Yang JH (2014), "Comparison of Blast-Induced Damage Between Presplit and Smooth Blasting of High Rock Slope," *Rock Mechanics and Rock Engineering*, **47**(4): 1307–1320.

Hu YG, Lu WB, Wu XX, Liu MS and Li P (2018b), "Numerical and Experimental Investigation of Blasting Damage Control of a High Rock Slope in a Deep Valley," *Engineering Geology*, **237**: 12–20.

Huang JQ, Zhao M, Xu CS, Du XL, Jin L and Zhao X (2018), "Seismic Stability of Jointed Rock Slopes Under Obliquely Incident Earthquake Waves," *Earthquake Engineering and Engineering Vibration*, **17**(3): 527–539.

Hudaverdi T and Akyildiz O (2021), "An Alternative Approach to Predict Human Response to Blast Induced Ground Vibration," *Earthquake Engineering and Engineering Vibration*, **20**(1): 257–273.

Johnson GR and Holmquist TJ (1994), "An Improved Computational Constitutive Model for Brittle Materials," *AIP Conference Proceedings*, **309**: 981–984.

Karadogan A, Kahriman A and Ozer U (2014), "A New Damage Criteria Norm for Blast-Induced Ground Vibrations in Turkey," *Arabian Journal of Geosciences*, **7**(4): 1617–1626.

Leidig M, Bonner JL, Rath T and Murray D (2010), "Quantification of Ground Vibration Differences from Well-Confined Single-Hole Explosions with Variable Velocity of Detonation," *International Journal of Rock Mechanics and Mining Sciences*, **47**(1): 42–49.

Li HB, Xia X, Li JC, Zhao J, Liu B and Liu YQ (2011), "Rock Damage Control in Bedrock Blasting Excavation for a Nuclear Power Plant," *International Journal of Rock Mechanics and Mining Sciences*, **48**(2): 210–218.

Liu W, Miao HQ, Wang C and Li J (2020), "Test on a Buried Pipe Network Subjected to an Artifcial Earthquake Produced by Multi-Millisecond Blasting," *Earthquake Engineering and Engineering Vibration*, **19**(3): 791–810.

Ma GW and An XM (2008), "Numerical Simulation of Blasting-Induced Rock Fractures," *International Journal of Rock Mechanics and Mining Sciences*, **45**(6): 966–975.

Murthy VMSR and Dey K (2003), "Predicting Overbreak from Blast Vibration Monitoring in a Lake Tap Tunnel – A Success Story," *Fragblast*, **7**(3): 149–166.

Onederra IA, Furtuey JK, Sellers E and Iverson SR (2013), "Modelling Blast Induced Damage from a Fully Coupled Explosive Charge," *International Journal of Rock Mechanics and Mining Sciences*, **58**: 73–84.

Ouchterlony F, Sjorberg C and Jonsson B (1993), "Blast Damage Predictions from Vibration Measurements at the S.K.B. Underground Laboratories at Aspo in Sweden," *Proceedings of the 9th Annual Symposium on Explosives and Blasting Research*, San Diego, USA, pp. 189–197.

Sanchidrian JA, Castedo R, Lopez LM, Segarra P and Santos AP (2015), "Determination of the JWL Constants for ANFO and Emulsion Explosives from Cylinder Test Data," *Central European Journal of Energetic Materials*, **12**(2): 177–194.

Scarpato DJ (2016), "Constructibility Challenges for Perimeter Control Blasting and Slope Development in Shale and Other ''Weak'' Rocks," *Rock Mechanics and Rock Engineering*, **49**(2): 653–659.

Singh PK and Roy MP (2010), "Damage to Surface Structures due to Blast Vibration," *International Journal of Rock Mechanics and Mining Sciences*, **47**(6): 949–961.

Sun GH, Lin S, Cheng SG, Sui T, Li CG and Zheng H (2018), "Mechanisms of Interaction Between an Arch

Dam and Abutment Slope Using Physical Model Tests," *Rock Mechanics and Rock Engineering*, **51**(8): 2483–2504.

Verma HK, Samadhiya NK, Singh M, Goel RK and Singh PK (2018). "Blast Induced Rock Mass Damage around Tunnels," *Tunnelling and Underground Space Technology*, **71**(1): 149–158.

Wang R, Deng XH, Meng YY, Yuan DY, Xia DH (2019), "Case Study of Modified H-B Strength Criterion in Discrimination Of Surrounding Rock Loose Circle," *KSCE Journal of Civil Engineering*, **23**(3): 1395–1406.

Wang ZL, Li YC and Shen RF (2006), "Numerical Simulation of Tensile Damage and Blast Crater in Brittle Rock Due to Underground Explosion," *International Journal of Rock Mechanics and Mining Sciences*, **44**(5): 730–738.

Xia WJ, Lu WB, Wang GH, Yan P, Liu D and Leng ZD (2020), "Safety Threshold of Blasting Vibration Velocity in Foundation Excavation of Baihetan Super-High Arch Dam," *Bulletin of Engineering Geology and the Environment*,**79**: 4999–5012.

Yan P, Lu WB, Zhang Jing, Zou YJ and Chen M (2017), "Evaluation of Human Response to Blasting Vibration from Excavation of a Large Scale Rock Slope: A Case Study," *Earthquake Engineering and Engineering Vibration*, **16**(2): 435–446.

Yan P, Zou YJ, Lu WB, Hu YG, Leng ZD, Zhang YZ, Liu L, Hu HR, Chen M and Wang GH (2016), "Real-Time Assessment of Blasting Damage Depth Based on the Induced Vibration During Excavation of a High Rock Slope," *Geotechnical Testing Journal*, **39**(6): 991–1005.

Yang JH, Cai JY, Yao C, Li P, Jiang QH and Zhou CB (2019), "Comparative Study of Tunnel Blast-Induced Vibration on Tunnel Surfaces and Inside Surrounding Rock," *Rock Mechanics and Rock Engineering*, **52**(11): 4747–4761.

Yang JH, Dai JH, Yao C, Jiang SH, Zhou CB and Jiang QH (2020), "Estimation of Rock Mass Properties in Excavation Damage Zones of Rock Slopes Based on the Hoek-Brown Criterion and Acoustic Testing," *International Journal of Rock Mechanics and Mining Sciences*, **126**: 104192.

Yang R, Rocque P, Katsabanis P and Bawden WF (1994), "Measurement and Analysis of Near-Field Blast Vibration and Damage," *Geotechnical and Geological Engineering*, **12**(3): 169–182.

Yuan W, Liu SG, Wang W, Su XB, Li ZH, Li JX, Wen L, Chang JF and Sun XY (2019), "Numerical Study on the Fracturing Mechanism of Shock Wave Interactions Between Two Adjacent Blast Holes in Deep Rock Blasting," *Earthquake Engineering and Engineering Vibration*, **18**(4): 735–746.

Zeng YQ, Li HB, Xia X, Liu B, Zuo H and Jiang JL (2018), "Blast-Induced Rock Damage Control in Fangchenggang Nuclear Power Station, China," *Journal of Rock Mechanics and Geotechnical Engineering*, **10**(5): 914–923.

Zhou CB, Jiang QH, Wei W, Chen YF and Rong G (2016), "Safety Monitoring and Stability Analysis of Left Bank High Slope at Jinping-I Hydropower Station," *Quarterly Journal of Engineering Geology and Hydrogeology*, **49**(4): 308–321.